ELSEVIER

Agricultural and Forest Meteorology 95 (1999) 113–137

AGRICULTURAL AND FOREST METEOROLOGY

Frost risk mapping derived from satellite and surface data over the Bolivian Altiplano

C. François[1,a,*], R. Bosseno[a], J.J. Vacher[a], B. Seguin[b]

[a]*ORSTOM, CP 9214, La Paz, Bolivia*
[b]*INRA Bioclimatologie, 84914, Avignon Cedex 9, France*

Received 29 December 1997; accepted 13 November 1998

Abstract

Summer frosts occur frequently on the Bolivian Altiplano (4000 m) and cause severe damage to potato and quinua crops. A regional statistical study of frost risks must combine meteorological data with satellite data. In this work, a new method is developed to use NOAA satellite temperatures together with local minimum air temperature data. This method enables point meteorological data (with important historical records) to be combined with satellite data (spatially extended but with poor temporal coverage). The method involves several stages including a classification of the Altiplano based on the meteorological stations, a calculation of minimum temperatures over the whole Altiplano for several years of data, and finally the computation of minimum temperatures and frost risk percentage maps. The precision obtained in the resulting synthesis images is 0.8°C for the average minimum temperatures and 9% for frost risk maps.

Keywords: Frost; Agro-climatic mapping; Radiative cooling; Potato; Remote sensing

1. Introduction

The Bolivian Altiplano, located at an altitude ranging from 3650 to 4300 m, covers 100 000 km^2 and has 250 000 rural inhabitants, more than one-quarter of the Bolivian rural population. The main crops are potato, bitter potato and quinua. They are essentially destined for subsistence farming with occasional surplus for the market. Climate is the most limiting factor for agricultural production: radiative frost risks during the growing period, low and irregular precipitation – with high risks of drought during the cultivating period – are observed (Le Tacon, 1989).

Most frosts occurring on the Altiplano throughout the year are radiative frosts, generated by radiation exchanges with the cold night sky. This study focuses on the frost risks during the cultivating period (October–April). The crucial agricultural period for frost occurrence is January, February and March, when crops are growing. During these 3 months, frost risk is not at its peak but may cause severe damage to crop yield. From observations and bibliographical study it appears that common potatoes (*Solanum tuberosum*, *Solanum tuberosum ssp andigena*) cannot withstand temperatures lower than −2°C (or −3°C for the most resistant ones). Bitter potatoes and quinua, on the other hand, can withstand temperatures as low as −5°C (Le Tacon, 1989; Allirol et al., 1992).

Frost occurrence in January/February varies considerably from year to year (Le Tacon et al., 1992),

*Corresponding address. Tel.: +33-3925-4905; fax: +33-3925-4922; e-mail: francois@cetp.ipsl.fr

[1]CETP, 10, 12 avenue de l'Europe, 78140 Vélizy, France.

0168-1923/99/$ – see front matter
PII: S0168-1923(99)00002-7

making it necessary to carry out a statistical study involving numerous years of data. Such long series of data are only available for 17 meteorological stations on the Altiplano: these data records include minimum night temperature, which generally occurs around 6.00 a.m., just before sunrise. In order to be able to have frost information over the whole Altiplano, global coverage using satellite data is necessary. In this study, infrared temperature data from AVHRR/NOAA are used. The goal of this paper is to extend the meteorological stations' historical data records (about 30 years of monthly minimum temperatures) to the whole Altiplano and thus obtain a statistical zoning based on frost risks. The resulting products are frost risks maps for potato and quinua crops over the Altiplano. These maps will help to plan a large-scale frost protection campaign.

We present a method that takes advantage of the temporal information given by the meteorological stations as well as the spatial information given by the satellite. In our case practical limitations arise which limit the usable dataset: no satellite image is useful in January/February due to the considerable cloud cover during this period (rainy season), and only 2 years of satellite data are available: 1995 and 1996.

A bibliographical review on the possibilities of using remote sensing data in order to perform frost mapping is presented in Kerdiles et al. (1996). As suggested by these authors, air temperatures will be used instead of surface temperatures (even if the latter are closer to the true physiological conditions) in order to establish a link with previous studies (Seguin et al., 1981): air temperatures have been used up to now in classical agrometeorological studies. The main advantage of using minimum air temperatures instead of minimum surface temperatures is that minimum air temperatures are more frequently (and easily) measured in agrometeorological stations. Recent studies, such as Santibañez et al. (1998), use the same approach.

2. Presentation and principles of the study

2.1. Available data

Seventeen meteorological stations over the Altiplano are used for this study. The five stations used for subsequent validation appear in white (see Fig. 1). The Bolivian Altiplano (18°S, 68°W, altitude: 4000 m) is bounded to the north by Lake Titicaca, to the south by the Uyuni Salar, to the west by the Oriental Cordillera and to the east by the Real Cordillera (see Fig. 1(b)). Lake Titicaca and its surroundings are the rainier and warmer part of the Altiplano (Fig. 1), and thus the most cultivated area. The southern Altiplano is a cold, dry and very low cultivated region.

For each station, the monthly minimum air temperature is available for the past 10–47 years (depending on the length of the record for the station) with an average of 30 years (see Table 1). For recent years (and especially 1995–1996) we have also at our disposal the daily nocturnal minimum temperatures for each station.

Moreover 25 clear night AVHRR images are available over the Altiplano (taken between 2.00–3.00 a.m.), from April 1995 to May 1996 (see Table 2). Each image, after cloud cleaning, atmospheric corrections and georeferencing, provides surface temperatures for the pixels of each station and date, and for the Altiplano as well. Nevertheless, no study related to frost occurrence can be undertaken using directly this set of satellite images because the months of interest (January and February) are missing (see Table 2), due to cloud cover. Also no long-term frost statistics can be derived using only 2 years of data (i.e. only two occurrences for January and February).

Since we are working with infrared satellite data, we are mainly interested in radiative frost occurrences that are likely to occur on clear and calm nights, rather than advective frost occurrences, resulting from the incursion of cold air masses, which are likely to occur on windy and cloudy nights. Whenever a clear satellite image is available, we use it to seek a correlation between night surface temperatures and air temperatures, without prejudging the nature of the frost.

2.2. Different nature of meteorological and satellite data

The differences between minimum meteorological temperature (T_{min}) and satellite temperature (T_s) are of three types: a time difference (6 a.m. for minimum night temperature versus 2 a.m. for satellite temperature), a height difference (1.5 m air temperature for

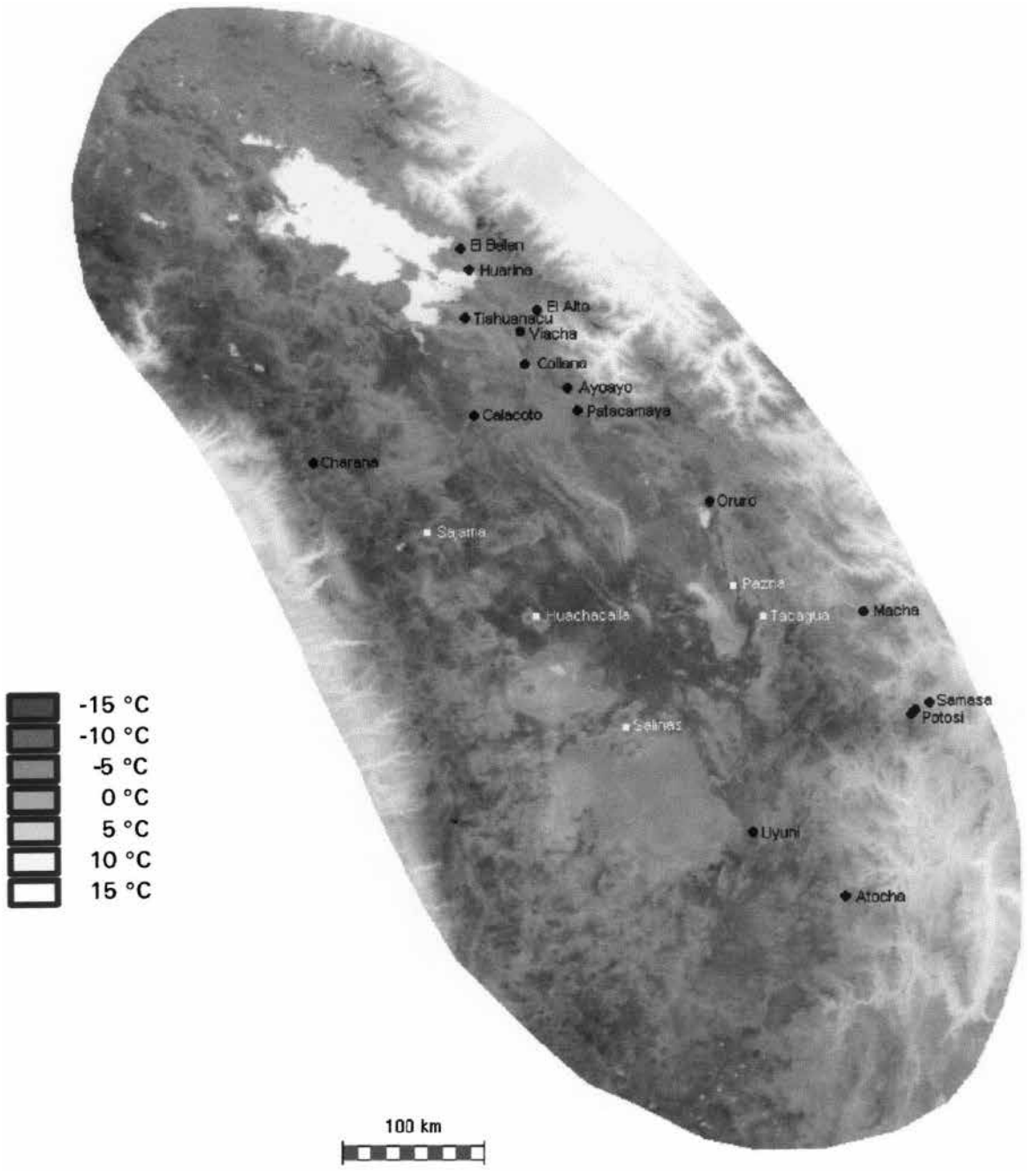

Fig. 1. (a): Night thermal infrared NOAA/AVHRR image (28 April 1995, chanel 4): the Altiplano and the meteorological stations. The classification stations appear in black, the validation stations in white (b): Map of the Bolivian Altiplano between the eastern and western cordillera. The principal features are indicated.

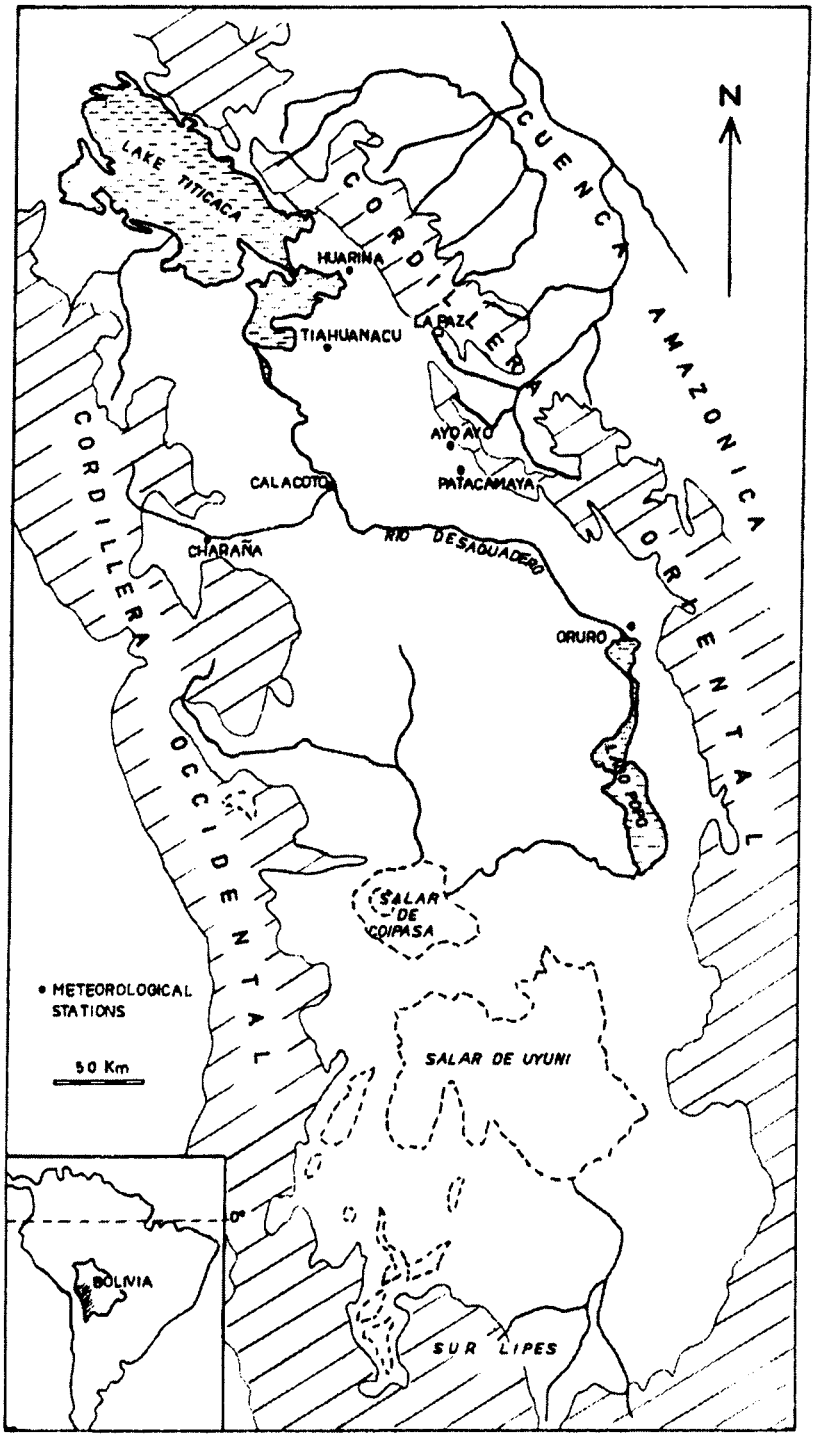

Fig. 1 (*Continued*).

Table 1
List of the 17 meteorological stations, together with the length of the meteorological data records

Name of the station	No. of years of data	Latitude (S)	Longitude (W)	Altitude (m)
Ayo Ayo	32	68°00′	17°05′	3856
Calacoto	22	68°38′	17°16′	3805
Charana	44	69°43′	17°35′	4057
Collana	22	68°17′	16°54′	3940
El Alto	47	68°11′	16°30′	4057
El Belen	37	68°41′	16°01′	3820
Huarina	20	68°38′	16°11′	3825
Patacamaya	24	67°56′	17°15′	3789
Tiahuanacu	18	68°40′	16°33′	3629
Viacha	26	68°18′	16°39′	3850
Oruro	47	67°00′	17°59′	3701
Atocha	10	66°13′	20°56′	3700
Macha	12	66°01′	18°49′	3480
Potosi	47	65°45′	19°35′	3945
Potosi (airport)	13	65°44′	19°32′	4100
Samasa	10	65°41′	19°29′	3650
Uyuni	23	66°50′	20°26′	3660

Table 2
List of the 25 available satellite images (AVHRR), year 1995–1996

Date	Local time (a.m.)	View angle	
		Maximum	Minimum
15 April 1995	2.20	23°	7°
28th April 1995	1.41	45°	29°
6 May 1995	1.55	32°	16°
12 May 1995	2.31	39°	23°
23 May 1995	2.13	9°	0°
31 May 1995	2.27	33°	17°
14 June 1995	1.36	47°	31°
24 June 1995	1.29	52°	35°
27 June 1995	2.37	48°	31°
7 July 1995	2.30	37°	21°
21 July 1995	1.39	47°	31°
25 July 1995	2.37	45°	29°
9 August 1995	1.35	48°	32°
19 August 1995	1.27	52°	36°
25 August 1995	2.03	26°	10°
25 September 1995	1.30	52°	35°
8 October 1995	2.31	33°	17°
20 October 1995	2.01	33°	17°
5 November 1995	2.30	29°	13°
6 March 1996	2.15	14°	0°
13 March 1996	2.40	41°	24°
24 April 1996	1.46	48°	32°
13 May 1996	1.41	51°	34°
18 May 1996	2.27	14°	0°
26 May 1996	2.41	36°	20°

meteorological data versus surface temperature for satellite data), and a spatial resolution difference (10–100 m^2 for station temperatures versus 1 km^2 for satellite temperatures).

Despite these differences it is possible to find a good correlation between satellite and minimum meteorological temperatures for each station, using the 2 years of data. This allows us to obtain – only for the pixel stations at this stage – the minimum air temperature T_{min}, using the pixel surface satellite temperatures T_s after atmospheric correction, whatever the date. This relationship between meteorological and satellite temperatures has three effects: it relates surface temperatures to 1.5 m air temperature, 2 a.m. temperatures to 6 a.m. minimum temperatures, and pixel temperature to station temperature.

2.3. Methodology

In short, the principle of the method is to obtain a set of relationships allowing us to create images from only 17 data points.

After image processing (Section 3), correlation and regression fits are performed for each station using 11 to 18 dates (out of the 25 available) depending on the cloud cover over the images. Linear

relationships between T_{min} and T_s are computed for each station (Section 4). This is the first step of the process.

In order to extend the previous relations to the whole Altiplano, a classification of the Altiplano based on the stations is necessary: the second step is therefore to determine the area of extrapolation of each station, that is, to classify the Altiplano in 17 areas according to the 17 stations. This is made by the calculation of the correlation between the surface temperature of each pixel of the Altiplano and the surface temperature of the 17 pixel stations, using the 25 dates. The pixel is assigned to the class corresponding to the station giving the best correlation. This is made using only satellite temperatures. For each pixel over the Altiplano, a new relationship is obtained between pixel temperature and the temperature of the corresponding station.

The last step is to extend the relationship between satellite temperatures to a relationship between minimum temperatures. With this new relationship, it is possible, knowing only the 17 minimum temperatures of the stations, to derive a synthesis image of minimum temperatures for the whole Altiplano. With this set of pixel-to-pixel relationship the historical data records, originally available only for the stations, are extended to the whole region. We thus create several images of monthly minimum temperatures for January, February and March between years 1946 and 1993 (depending on the stations). It is then possible to use these composite images to compute statistics about frost risks.

3. Image processing

3.1. Cloud identification

Although most of the satellite images are cloud-free, some remaining clouds are present on some images. To identify these cloudy regions, the algorithm of Saunders and Kriebel (1988) is used. For each image, a threshold on AVHRR channel 5 (12 μm) is chosen in order to exclude large clouds, and a threshold on the difference between channel 4 (11 μm) and channel 5 (12 μm) is applied to exclude thin cirrus. After this identification, all clouds are flagged and no treatment is applied to these pixels.

3.2. Atmospheric corrections

The water vapour-dependent (WVD) Split-Window algorithm is used to perform atmospheric corrections on the images (François and Ottlé, 1996). Each coefficient is quadratic in W:

$$T_s = (a_1W + a_2W_2 + a_3)T_{b11} + (b_1W + b_2W_2 + b_3)T_{b12} + (c_1W + c_2W_2 + c_3) \quad (1)$$

where W is the water vapour content, T_s is the corrected surface temperature, T_{b11} and T_{b12} the channel 4 (11 μm) and 5 (12 μm) brightness temperatures, and $a_1,\ldots,a_3,b_1,\ldots,b_3,c_1\ldots,c_3$ are the Split-Window coefficients. The water vapour content W is calculated on 40×40 pixels squares over the image using the variance–covariance method proposed by Sobrino et al. (1993) and developed by Ottlé et al. (1997).

The relative accuracy of the temperatures obtained through the atmospheric correction process is estimated to be better than 1 K, and even better for the very dry atmospheric conditions of the Altiplano (François and Ottlé, 1996).

One may note that the determination of true *surface* temperatures (adjusted for surface emissivity) is not necessary since a good correlation is obtained using atmospheric-corrected satellite *brightness* temperatures (and not satellite *surface* temperatures): therefore, the determination of surface emissivity is not necessary (and impossible in fact with our dataset). Assuming that no important temporal variation of surface emissivity occurred, Split-Window coefficients corresponding to a constant surface emissivity is chosen ($\varepsilon = 1$). In reality, the emissivity of a given pixel may change throughout the year, from 0.92 to 0.93 for a bare soil to 0.99 for a fully vegetated area (which is not likely to occur over the Bolivian Altiplano). The variation in T_s due to a variation in ε is nearly linear and a calculation for the specific conditions of the Altiplano give the following expression (see Appendix A):

$$\Delta T_s \approx 20\Delta\varepsilon$$

A (possible) variation of 0.02 in emissivity during the year would therefore lead to a typical variation of 0.4°C in the surface temperature derived from satellite. This is the second source of error in the scheme, the first one being the error related to atmospheric corrections.

3.3. Georeferencing

After these corrections, the last step before obtaining surface satellite temperatures for each meteorological station is to georeference each AVHRR image to obtain coincident images and to be able to locate the position of each meteorological station. The resulting precision obtained by georeferencing is better than one pixel (1 km^2). Using the geographical and topographical location of the stations, 3 × 3 pixel masks are determined for each station to calculate the mean corrected surface temperature: on plains, the 9 pixels of the square are used to compute the mean value, although near hills or lakes, for instance, only the 3 or 4 pixels considered to be representative of the station are used.

4. Correlation between minimum air temperature and satellite surface temperature for each station

4.1. Comparison of in situ and satellite data

After georeferencing, we are able to compare satellite temperatures T_s with nightly minimum station temperatures T_{min} for each station. Fig. 2 shows the

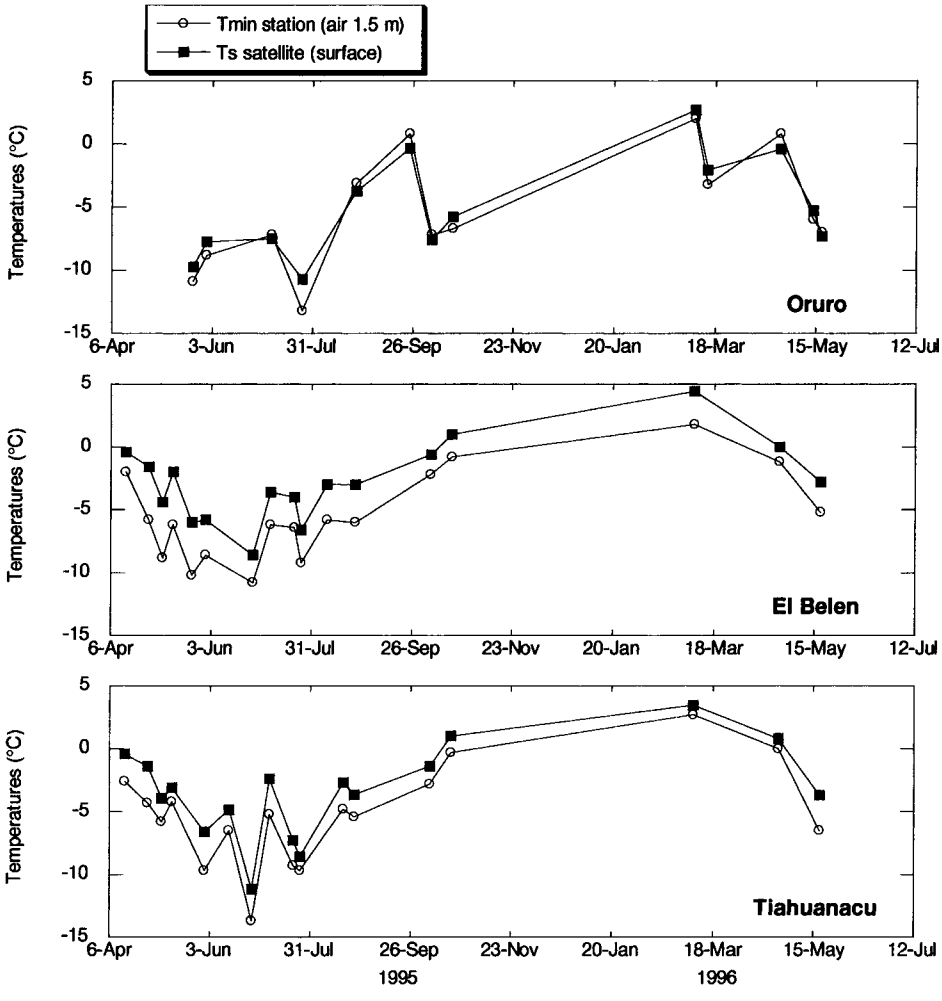

Fig. 2. Comparison between minimum air temperature (T_m) and surface satellite temperature ($T_{s)}$ (in °C) for three stations (Oruro, El Belen, Tiahuanacu) over the Altiplano from April 1995 to May 1996.

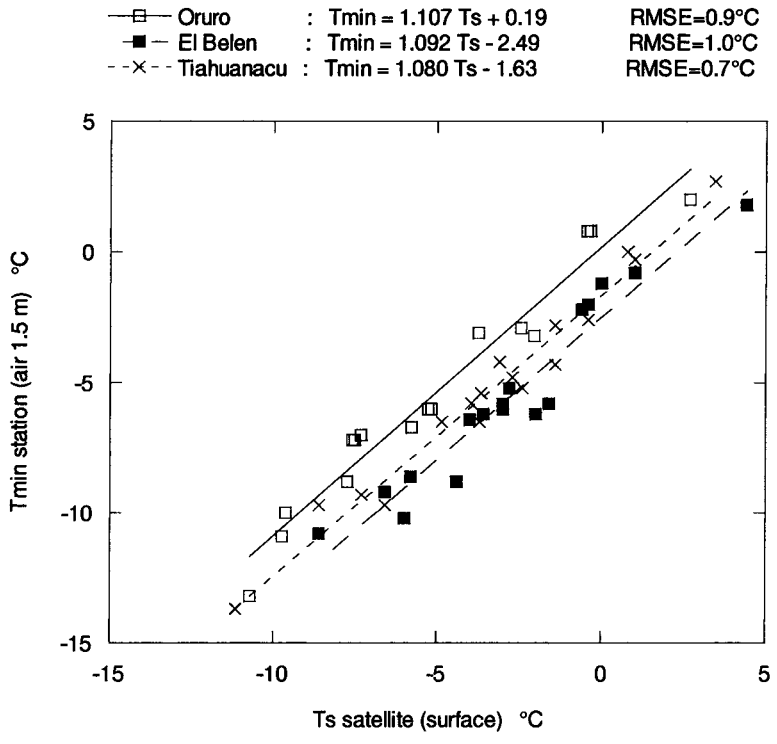

Fig. 3. Regression fits between T_s and T_{min} for the three stations (Oruro, El Belen, Tiahuanacu). Correlation coefficient R is given together with RMSE.

plots of T_s and T_{min} for three stations (namely Oruro, El Belen, and Tiahuanacu). Although both satellite and station temperatures are very different in nature (see Section 2.2), one may note that the temperatures are well correlated, which allows us to derive regressions between T_s and T_{min} (see Fig. 3). This good correlation between air temperature and surface temperature is presumably due to the fact that most frosts occurring on the Altiplano are radiative frosts, when the surface is cooling the air above.

An interesting fact is the variation of the relation among the different stations. Two opposite effects are involved. The first effect is due to the time difference: T_{min} (6 a.m.) is cooler than T_s (2 a.m.). The second effect, due to the height of measurement, has an opposite effect: T_s (surface temperature) is cooler than T_{min} (1.5 m air temperature). For two stations (El Belen, Tiahuanacu) T_s is higher than T_{min} (the first effect is the most important). For the other one (Oruro), both temperatures are quasi-equal (the two effects compensate each other).

Another effect has to be taken into account: spatial resolution also plays a role in the difference between air and surface temperature, according to the position of the station with respect to the surrounding pixel. The station of Ayo Ayo, for instance, is located in a basin, and thus, at the same time, station temperature is lower than pixel temperature. This increases the first effect, and therefore, the difference between both temperatures is greater for Ayo Ayo than for other stations (see Table 3).

Table 3 presents the regression fit relations for all stations, together with standard deviation and the number of points used. It appears clearly that, although the relations are similar, there are some differences among the stations.

The fourth column in Table 3 shows that the regressions are based on a maximum of 18 points and a minimum of 11 points. Therefore, from 7 to 14 points have been eliminated, for different reasons: clouds, large satellite angle (low spatial resolution and fuzzy image), or human reasons (imprecision

Table 3
Regression relations between T_s and T_{min} for each meteorological station

Name of the station	Relation T_{min}/T_s	RMSE(°C)	Correlation coefficient R	No. of images used
Ayo Ayo	$T_{min} = 1.130\ T_s - 3.15$	0.9	0.98	14
Calacoto	$T_{min} = 1.057\ T_s - 1.41$	0.9	0.98	15
Charana	$T_{min} = 1.109\ T_s + 1.62$	1.0	0.94	11
Collana	$T_{min} = 1.074\ T_s + 0.37$	0.9	0.95	17
El Alto	$T_{min} = 1.042\ T_s + 0.18$	0.9	0.95	18
El Belen	$T_{min} = 1.092\ T_s - 2.49$	1.0	0.96	17
Huarina	$T_{min} = 0.937\ T_s - 1.24$	0.8	0.96	11
Patacamaya	$T_{min} = 1.140\ T_s - 0.69$	1.0	0.98	13
Tiahuanacu	$T_{min} = 1.080\ T_s - 1.63$	0.7	0.98	17
Viacha	$T_{min} = 0.893\ T_s - 3.96$	0.9	0.96	14
Oruro	$T_{min} = 1.107\ T_s + 0.19$	0.9	0.98	16
Atocha	$T_{min} = 0.911\ T_s + 0.92$	1.0	0.98	12
Macha	$T_{min} = 1.130\ T_s - 0.23$	1.0	0.95	11
Potosi	$T_{min} = 0.967\ T_s - 1.00$	0.8	0.94	14
Potosi (airport)	$T_{min} = 0.872\ T_s + 0.51$	0.7	0.95	15
Samasa	$T_{min} = 1.000\ T_s + 0.96$	0.7	0.97	15
Uyuni	$T_{min} = 1.014\ T_s + 2.33$	0.7	0.99	16

in the meteorological records). The mean RMSE obtained, 0.9°C, is acceptable for our purpose, and similar to the accuracy of T_s estimation.

The relations obtained may be used to derive minimum temperatures from satellite temperatures. However, these relations have not been derived for the whole Altiplano, but for the 17 isolated stations. In order to attempt to obtain a global relation, we combined all the data from all stations to derive a global fit. Despite the similarity between the relations, accuracy was perceptibly lowered (RMSE was found to be 1.8°C). It seems clear that each station, due to its geographical situation, type of soil, topography, relief, etc., presents a particular behaviour. We tried to introduce a linear relation involving the amount of vegetation to improve the relation since cooling during the night is usually greater for vegetated surfaces than for bare soils. Therefore a vegetation index (NDVI) was computed from AVHRR visible and near-infrared channels: 45-day images throughout the year 1995–1996 were used. No correlation was found between the cooling and the NDVI with our data. No improvement was observed in the relationship when NDVIs were introduced. The probable explanation is that vegetation cover, as a cooling factor, is important from sunset to 0 a.m., but almost negligible after 1 a.m. (Cellier, 1989 and pers. comm.). Since satellite images are taken after 1.30 a.m., vegetation amount has no significant influence in our case.

A classification of the Altiplano is therefore necessary to make correct use of the different relations: each relation should be used in an area having the same behaviour as the corresponding station.

5. Spatial extrapolation of minimum temperatures

The detailed methodology for the derivation of minimum temperature maps from pin-point station temperatures is described in Appendix B: four spatial functions, f, g, f' and g' are been defined to represent the different ways of linking T_m to T_s, and station temperatures to pixel temperatures. Our purpose is to determine function g which enables us to extrapolate the meteorological temperatures data (available only at the stations) to the whole Altiplano. In order to calculate g, we need first to determine f', g' and f (see Appendix B).

5.1. Classification of the Altiplano based on the stations: Determination of function g'

The classification of the Altiplano is necessary to extend the preceding relation f' linking T_s to T_{min}, to

the whole Altiplano (function f): since we cannot use a global relation for the whole Altiplano, we use 17 relations applied to 17 *zones*, corresponding to the 17 stations. These zones are determined using a regression between the surface temperature of the ith station $T_s(x_i, y_i)$ and any pixel $T_s(x, y)$. This is the definition of function g' (see Appendix B).

The same dates used in Section 4 are selected to perform the regression between $T_s(x_i, y_i)$ and $T_s(x, y)$. The same 3×3 squares are also used. The procedure is repeated over the whole Altiplano, station by station. For a given pixel (x, y), if no satellite data are available for a selected date (e.g. cloudy pixel), the date is eliminated. If there are more than five dates to perform the regression the correlation coefficient R and regression coefficients α and β are stored for this pixel (x, y).

Finally 17 'images' of correlation coefficients are obtained. For each pixel, the best correlation coefficient is chosen. If the resulting maximum correlation R is greater than 0.84 (i.e. $R^2 > 0.70$), the corresponding station i is assigned to the pixel (x, y), otherwise the pixel is flagged as unassigned and not used for further processes. These rejected pixels generally correspond to lakes and salars, and represent less than 2% of the total pixel number. The resulting image is a classification of each pixel of the Altiplano according to the stations. This classification map is given in Fig. 4. Each colour represents a station. Black pixels are unassigned pixels. This map does not have a particular significance for frost risks: it just means that the temperatures of some pixels are related with the temperature of a given station by a linear relationship (which is different for each pixel), and this is a kind of visualisation of function g'.

5.2. Spatial extrapolation: Determination of function f and g

Function f, which is the function that generalises function f' to the whole Altiplano, can now be derived using the above-described classification: it is assumed that for a given station i, f_i' may be generalised to the whole zone corresponding to this station. This assumption may be discussed, but seems reasonable since all relationships f_i' are close to each other. Moreover, it appears to be a better solution than taking a single function for all the Altiplano. Therefore, for

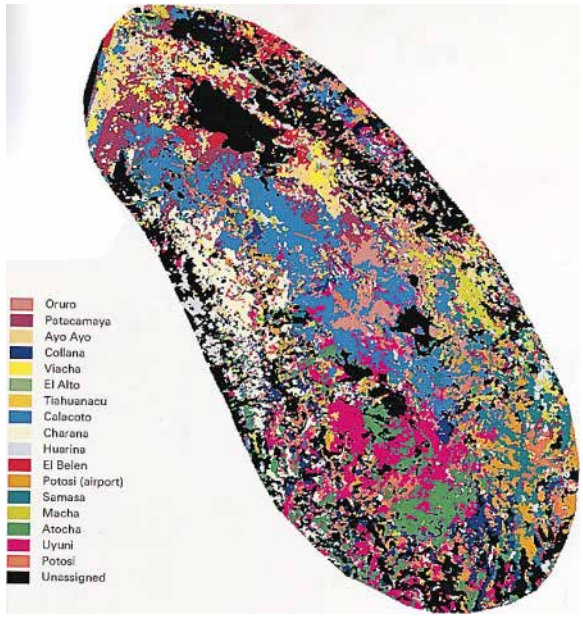

Fig. 4. Classification of the Altiplano based on the stations. Each colour corresponds to the zone attached to a given station.

each zone i embedding the pixels (x, y) linked to the ith station, f may be determined by $f(x, y) = f_i'(x, y)$, which can be written in symbolic form as $f = f'$. This hypothesis is supported by the accuracy of the obtained results (see Section 6). However this hypothesis is evaluated more directly using the cross-validation technique (see Section 5.3).

We are now able, through f, to compute minimum temperatures from an image of satellite temperatures. This is useful for instant frost diagnosis. Using the relationships given in Table 3, together with the classification map given in Fig. 4, it is possible to derive minimum temperatures at 6 a.m., with an image taken at 2 a.m.

Nevertheless, the principal goal of this study is to know function g to derive minimum temperature maps from point meteorological stations. The 30 years of very localised data records can be extended to the whole region using function g. This function g may be calculated as shown in Appendix B:

$$g = f(g(f^{-1})) \tag{2}$$

The classification based on the stations together with the functions f and g' are used to calculate coefficients of the function g for each pixel (x, y).

At this point, we have at our disposal a set of point historical data $T_{min}(x_i, y_i)$ (from 10 to 47 years of data, depending on the stations) and a function to compute $T_{min}(x, y)$ on each pixel of the Altiplano.

5.3. Cross-validation of the scheme using the daily 1995–1996 data

In order to evaluate the errors associated with the different assumptions made in the scheme, two types of statistical cross-validations is performed, on a daily basis, using the 1995–1996 satellite images and daily minimum temperatures. Cross-validation is a technique to estimate the forecast skill of a statistical forecasting model (Michaelsen, 1987). The cross-validation method systematically deletes one case in a dataset, computes a forecast model from the remaining cases, and tests it on the deleted case.

5.3.1. Temporal stability and spatial accuracy

The first cross-validation test is applied to the prediction of the field of satellite temperatures using the observed point thermometer temperatures. In this case, the analysis has been repeated 25 times, each time withholding one of the AVHRR images in the fitting, and then predicting that image from the resulting regression. This test allows us to test the temporal stability of the scheme as well as its spatial prediction ability. Both points are important: (a) Temporal stability: it is implicitly assumed in the scheme that the relationships derived for months of April–May 1995 also apply to the months of January and February 1996 (which are missing from the series of satellite data, and which are the months for which the relationships are required). It is important to test if the scheme is able to predict the field of temperatures for a date that is not part of the fitting scheme. It is important to note here that it is also assumed in the scheme that the relationships derived using the 1995–1996 data also apply for years 1946–1993. (b) Spatial prediction skill: this first cross-validation test also involves the test of the $g'(f^{-1})$ part of the scheme (see Appendix B), which is related to the spatial extension of the point temperatures to the whole Altiplano (function g').

The results are presented in Table 4: the difference between predicted and measured satellite temperature is calculated for each pixel of the Altiplano. The whole image, excluding Lake Titicaca and the Salars, contains 114 794 pixels. The resulting mean difference (bias) and the standard error is given for each date. The dates in italics in Table 4 correspond to very low quality images and are eliminated from the global comparison (last line on Table 4). These images are characterised by clouds (including undetectable thin cirrus) and/or high viewing angles, resulting in a very hazy aspect. On the contrary, some images are highlighted (in bold) for their remarkable quality, the Altiplano being very clear (unclouded) and/or sharp (viewing angle near to nadir) for these dates: the bias and standard error are always good for such dates.

Table 4
Comparison of simulated against measured satellite minimum temperatures

Deleted date (predicted image)	No of pixels	Bias (°C)	SE (°C)
15 April 1995	114 794	−0.5	1.9
28 April 1995	114 794	−0.3	1.8
6 May 1995	114 794	−0.9	2.2
12 May 1995	114 794	−0.3	1.3
23 May 1995	114 794	−0.9	1.9
31 May 1995	114 794	−0.3	1.8
14 June 1995	114 794	−0.2	2.8
24 June 1995	97 073	−0.1	3.4
27 June 1995	114 794	0.8	2.6
7 July 1995	114 794	1.4	4.4
21 July 1995	108 677	0.9	4.7
25 July 1995	108 629	1.4	1.8
9 August 1995	100 158	3.9	6.8
19 August 1995	100 413	2.6	5.2
25 August 1995	108 677	0.2	1.6
25 September 1995	93 395	4.4	7.2
8 October 1995	114 794	1.1	3.2
20 October 1995	114 794	−0.6	2.5
5 November 1995	100 361	0.4	3.8
6 March 1996	103 624	1.7	6.3
13 March 1996	68 795	−0.1	4.0
24 April 1996	109 663	0.6	3.7
13 May 1996	94 374	−0.2	2.8
18 May 1996	108 598	0.1	2.3
26 May 1996	83 998	1.3	2.5
Total	1 959 313	0.1	2.3

Withholding each of the 25 available dates in turn, data for the other 24 dates are used with the data from the 17 meteorological stations to predict the temperatures over the image area. The dates in italics correspond to low quality images (cloudy image with undetectable thin cirrus and/or large viewing angles and hazy aspect): these dates have not been taken into account in the total bias and standard error. Dates in bold correspond to very clear images (unclouded) and/or sharp images (viewing angle near to nadir).

The global result is quite good (a bias equal to 0.1°C with a standard error of 2.3°C) and shows that the algorithm is able to predict quite well a field of nearly 115 000 pixel from 17-point measurements. The low bias allows the algorithm to be used for average statistics such as frost statistic studies. The high standard error, on the other hand, shows that the algorithm is not accurate enough to be used for frost prediction on a daily basis.

Concerning temporal stability, few differences in the regression coefficients in f' are noted when one date is deleted. However, one important thing to be mentioned is that, logically, the performance of the retrieval is lowered when a particularly cold (24, 27 June and 25 July) or warm (8 October–11 November) date is deleted. The regression function f' should therefore be calculated with as wide a range of dates as possible.

5.3.2. Test of the global scheme

The second cross-validation test is applied to the prediction of nocturnal minimum temperatures using the 1995–1996 station data. For this test, each station is omitted in turn, and the procedure is applied to predict the minimum temperature of this station using the minimum temperature of its related station.

This test is performed on 12 stations only: five stations (Charana, Uyuni, Atocha, Macha and Potosi Airport) appear to have no related station (the correlation coefficient is always lower than 0.84) and would be represented as 'non-assigned' pixels in the scheme. Charana, for instance, is a very cold station situated in the western cordillera and could hardly be represented by another station (see Fig. 4). The same thing occurs, to a lesser extent, for the four other excluded stations which are rather atypical stations. This means that these five stations are very important in the scheme to represent atypical pixel behaviour (i.e. especially cold or warm pixels).

Since we have at our disposal both T_s and T_m for each station, we are able to test the prediction skill of each stage of the scheme, that is, each function in Eq. (2). The results are given in Table 5: at each stage of the scheme, the predicted temperatures are compared with the observed one (satellite temperature for Lines 1 and 2, and station temperature for Line 3). Table 5 is a summary of the scheme prediction skill, on a daily basis: each line represents the cumulative (and specific) error due to each step of the scheme. The first line represents the ability of function f'^{-1} to predict the satellite temperature of the cross-validation station from its minimum temperature. Not surprisingly we find a similar result to what was given in Table 3: a standard deviation of 0.9°C and a near-zero bias of 0.04°C. The second line represents spatial extension, that is, the ability of the scheme to predict the satellite temperature of the deleted station from the minimum temperature of the cross-validation station, that is, functions $g'(f^{-1})$. This test is analogous to the first test performed in Section 5.3.1. We find here a better result than what is found with the first cross-validation: a bias of 0.07°C and a standard deviation of 1.6°C. This is easily explained since this second test is applied on 17 stations on the central zone of the Altiplano, and not on 115 000 points over the whole region. The last line gives the total error for the whole scheme (including function f) on a daily basis: a bias of 0.2 and a standard error of 2.2°C.

The last column in Table 5 gives the specific error of each step: for this calculation, at each step, the computed temperature is replaced by the exact one, and the next step is predicted. It is possible in this way to evaluate separately the accuracy of functions g' and f (theoretical specific RMSE in Table 5). Function g' appears to cause an error of 1.4°C. Function f on its

Table 5
Comparison of predicted against measured minimum temperatures at 12 meteorological stations

	Bias	Cumulative RMSE	Real specific RMSE	Theoretical specific RMSE
f'^{-1}	0.04	0.9	0.9 (f'^{-1})	0.9 (f'^{-1})
$g'(f'^{-1})$	0.07	1.6	1.3 (g')	1.4 (g')
$f(g'(f'^{-1}))$	0.2	2.2	1.5 (f)	2.0 (f)

Each station in turn has been withheld and the minimum temperature for that station has been predicted from a combination of satellite data and the measurements from the remaining 11 meteorological stations.

own causes an error of 2.0°C: this is the error due to the assumption made to compute function *f*. The errors are not independent and actually slightly compensate each other: this is why the real specific errors (third column, calculated from the cumulative RMSE) are lower than the theoretical ones: 1.3°C and 1.5°C, respectively, for g' and *f*.

6. Frost risks mapping and resulting products: Derivation of statistical synthesis images

6.1. Resulting products

Being able to extend the historical data attached to each station to the whole Altiplano, the scheme is applied on monthly historical records in order to derive frost risk statistics. As noted in Section 2.1, the historical data contains monthly extreme minimum temperatures. The months of interest are January, February and March. These data are used together with function *g* to derive five types of maps:

– a map of extreme minimum temperatures (the extreme temperature of the considered period)
– a map of average minimum temperatures (the average of the extreme minimum temperatures)
– a map of frost risk percentages for potatoes
– a map of frost risk percentages for resistant potatoes
– a map of frost risk percentages for bitter potatoes and quinua

For a given station *i*, and for each year of the historical data record, the minimum temperature of January, February and March is calculated for each pixel of the zone *i* using function *g*. Thus, we obtain a new record of minimum temperatures for each pixel. It is then possible to calculate percentages, average or extreme temperatures on each new record, for each pixel of the Altiplano. Frost risk percentage is calculated as follows: it is the ratio of the number of years with a temperature lower than −2°C (for instance) divided by the total number of years in the data record.

For sake of clarity, temperature maps are divided into classes, including the threshold temperatures −2°C (potatoes), −3°C (resistant potatoes) and −5°C (bitter potatoes and quinua). These temperatures correspond to thresholds at vegetation level during the flowering stage, unlike the 1.5 m temperatures used in this study. A bibliographical and experimental study shows that the difference between plant temperature and air temperature is around 1°C for early morning frosts (Du Portal, 1993). The effective thresholds for percentage calculations are therefore −1°C for potatoes, −2°C for resistant potatoes, and −4°C for bitter potatoes and quinua, in terms of air temperatures. This difference does not change anything in the method and is used only to give more representative results for this application.

These five maps are derived for five different periods (covering the past 30 years on average, according to the considered zone, see Table 1 and Fig. 4):

January
February
March
January, February (minimum of January and February)
January, February, March (minimum of January, February and March)

The first maps are of interest to study frost occurrences from month to month, while the two last ones cover the cultivating period.

6.1.1. Minimum and average minimum temperatures maps

As an illustration, the map of extreme minimum temperatures in February is presented. The first observation when viewing the resulting map (Fig. 5) is that this synthesis image reproduces the geographical details of the Altiplano (see Fig. 1): the salt lakes, the hills and mountains all along the Altiplano appear clearly, as do the Corocoro hills between Calacoto and Oruro (see also Fig. 6 and Section 6.3), the two volcanoes near Huachacalla (see also Fig. 7 and Section 6.3) and the Sorata and La Paz valleys (which are the two warm, orange valleys that appear on the right side of Lake Titicaca).

A large cold region is observed in the centre of the Altiplano. One may note, in Fig. 5 that the warmer regions on the Altiplano are situated near Lake Titicaca, due to the particular microclimate that exists around the lake. To the South, the Coipasa and Uyuni salt lakes are also warmer than the surrounding area: this may be explained by the fact that the salt lakes are covered with water in January and February. The other

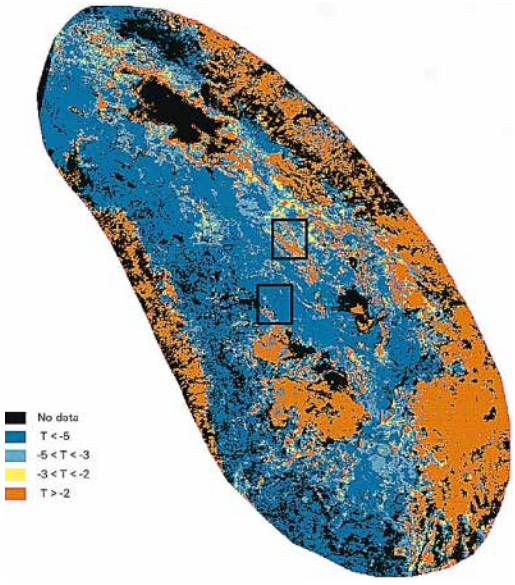

Fig. 5. Synthesis image of the Altiplano representing the extreme minimum temperatures over the past 30 years in February. The two rectangles indicate the areas shown enlarged in Figs. 6 and 7.

reason is the important thermal conductivity and thermal capacity of the Salars saline substratum. Local farmers have found that frost-sensitive crops can be cultivated near the Coipasa and Uyuni salt lakes. The other warm regions over the Altiplano between Lake Titicaca and Lake Poopo correspond to the hills. The last orange warm regions to the south and edges of the image no longer belong to the Altiplano and correspond to valleys.

The extreme minimum temperature maps are useful to have an idea of the extreme minimum temperatures that may occur on the Altiplano. It may be used to determine the regions where, for instance, potatoes may not be cultivated because temperatures always drop below -3°C, or the regions where potatoes may be cultivated with 100% chance of no frost, if the minimum temperature never drops below -2°C.

Average temperatures, on their own, give an idea of a 50% frost risk level (assuming the mean value equal to the median value): a zone with a mean temperature of -2°C is a zone with 15 nights of temperatures lower than -2°C and 15 nights with temperatures greater than -2°C.

Extreme minimum temperature maps and average minimum temperature maps, therefore, give useful information, but must be seen as complementary to frost risk maps, which encompass the information of each year of data.

Table 6
Surface area in km^2 (number of pixels) corresponding to the frost risk (%) and frost threshold (-2°C, -3°C and -5°C in terms of crop temperatures), in the January–February period

Frost risk in January–February (%)	-2°C	-3°C	-5°C
0–10	8 240	15 390	39 360
10–20	2 827	5 176	9 590
20–30	4 271	6 131	7 801
30–40	6 580	8 691	9 798
40–50	4 040	5 216	6 223
50–77	15 385	16 009	13 097
77–100	73 439	58 169	28 913

6.1.2. Frost risk maps

We present here a summary of the results obtained in the calculation of frost risk over the Altiplano. In this study, the real boundaries of the Altiplano are taken into account (warm valleys are excluded, so as the eastern and western cordilleras). Uncultivable zones such as lakes or salars are also removed from the statistics. In the end, a global surface area of 115 000 km^2 remains available. Table 6 presents the distribution of this global surface according to frost risk for the January–February period, over the past 30 years. Different thresholds are presented, in terms of crop temperature, corresponding to different possible cultivations: going from potatoes (threshold of -2°C) to resistant potatoes (threshold of -3°C), and finally bitter potatoes and quinua (threshold of -5°C). One may note immediately the extreme conditions of the Altiplano: the proportion of severe frosts occurring in summer remains significant: a major part of the Altiplano, 75 000 km^2, has a frost risk greater than 50% for potatoes or resistant potatoes, and makes cultivation very hazardous.

This table demonstrates the potential gain in cropping area, if, for instance, one changes the cultivation from potatoes (limit of -2°C) to resistant potatoes (limit of -3°C). In other words with one degree more in plant resistance, what surface do we gain? If the acceptable limit is fixed at a 10% risk, one can see on the first line of Table 6 that the obtained surface is almost twice larger than the former one, from 8240 to

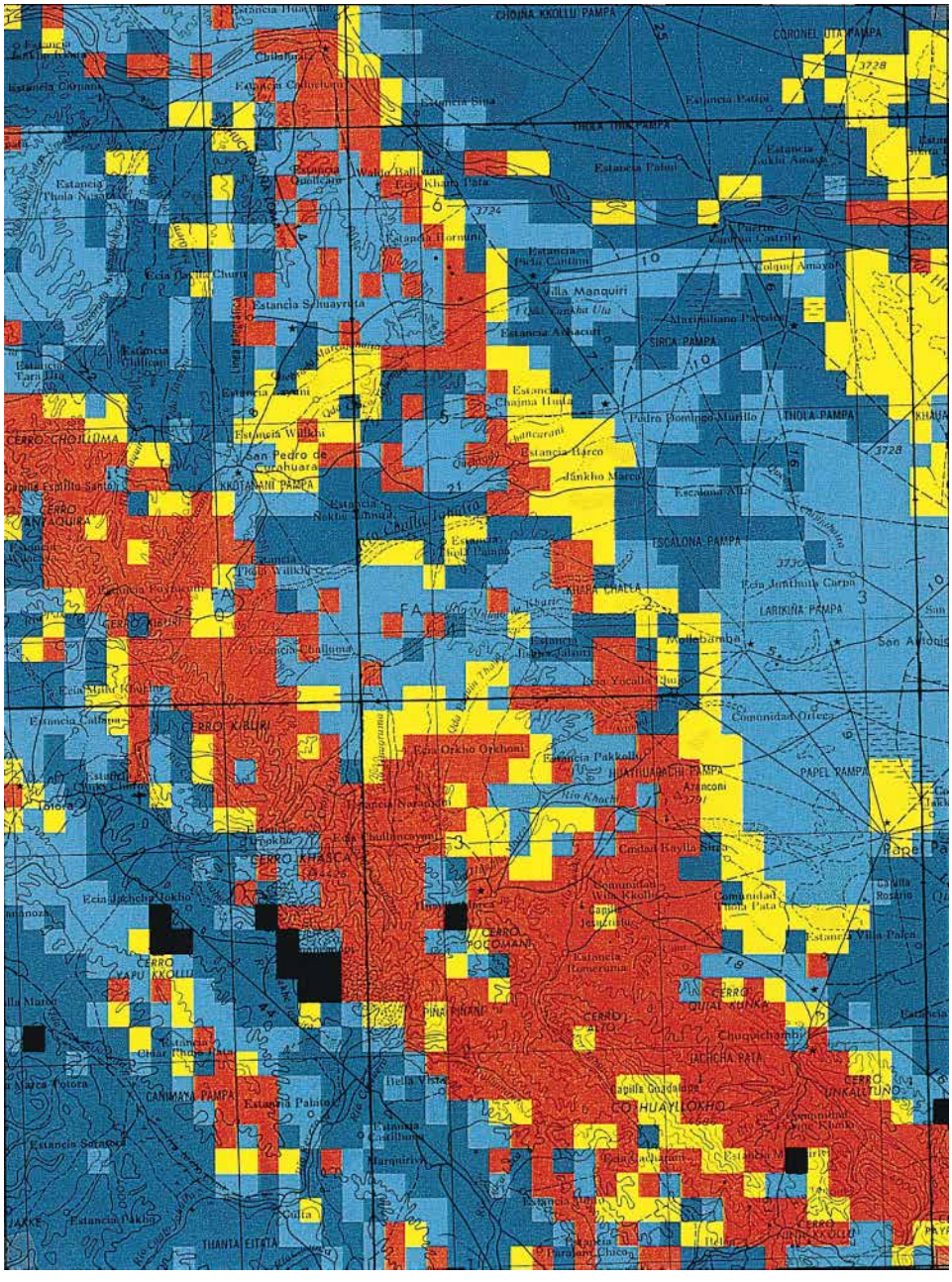

Fig. 6. Extreme minimum temperatures for the past 30 years in February for the Corocoro Hills region plotted over a map showing the altitude contours every 100 m. The area is shown as the upper rectangle in Fig. 5 using the same colour scale.

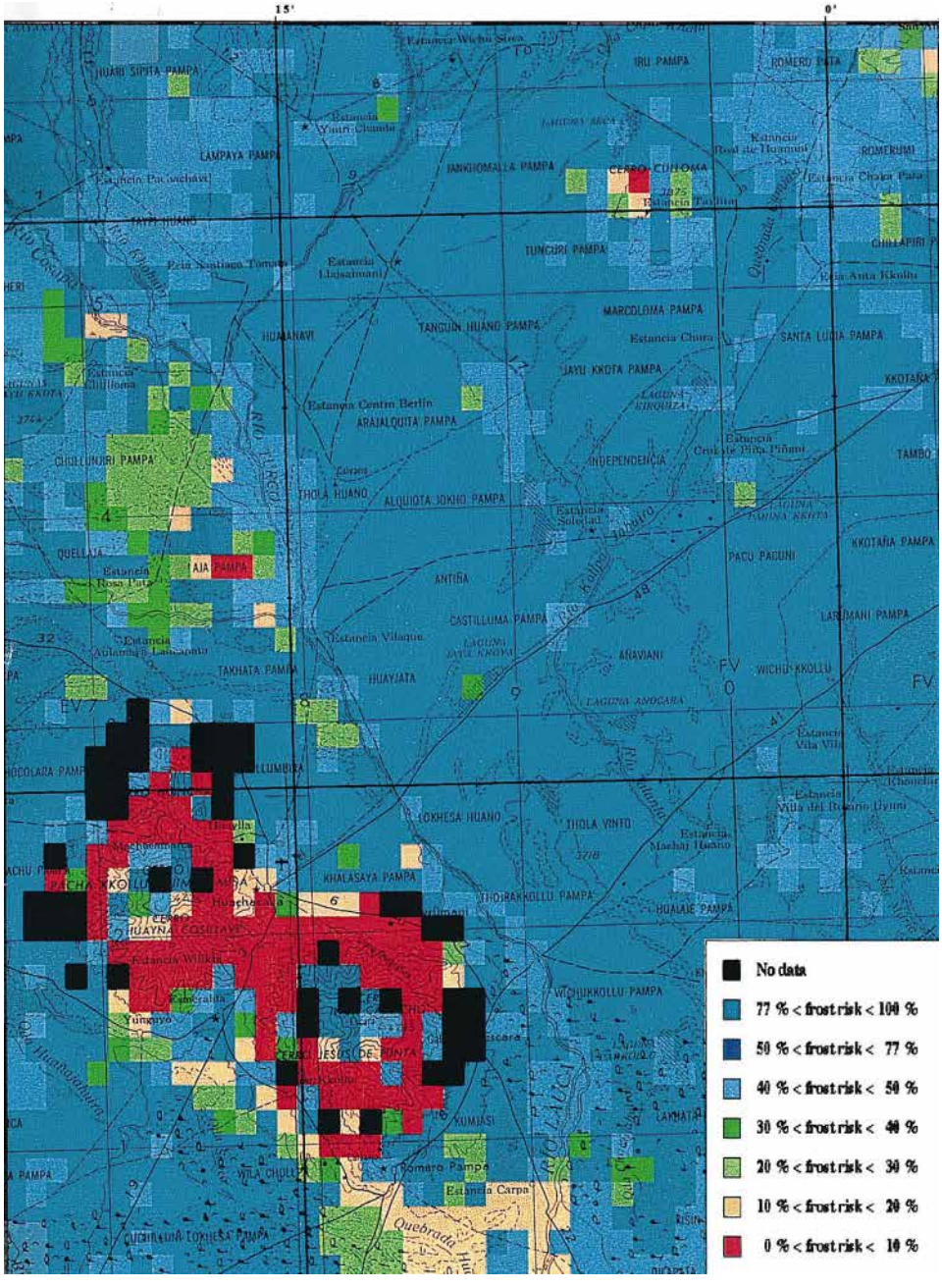

Fig. 7. Percentages for frost risks for potatoes over the past 30 years in February plotted over a map showing the altitude contours every 100 m. The area is shown as the lower rectangle in Fig. 5.

Table 7
Surface area in km^2 (number of pixels) corresponding to climatological frost risk (0°C in terms of air temperature) for different months

Climatological frost risk (0°C)	January	February	March	Jan–Feb	Jan–Feb–Mar
0–10%	6 114	5 730	2 189	4 616	2 020
10–20%	4 025	3 709	1 780	1 499	1 251
20–30%	7 269	3 882	1 300	2 262	1 341
30–40%	9 672	3 453	2 704	4 204	948
40–50%	4 180	3 775	5 886	2 429	1 449
50–77%	11 052	13 548	7 529	12 049	5 896
77–100%	72 470	80 685	93 394	87 723	101 877

15 290 km^2. This study could be performed on smaller and specific zones to evaluate precisely the gain, for instance, in changing culture from potatoes to quinua. Frost risk estimations could also be used to evaluate the interest of localised frost prevention campaigns. A precise application study, using daily or 10 days' data, could also be performed to statistically evaluate the probability and length of frost-free periods.

As an illustration, a detail of the frost risk map for potatoes (threshold of −2°C) in the February period is presented in Fig. 7 and detailed in Section 6.3.

Table 7 gives statistics related to climatological frost risk (0°C in terms of air temperature) which is of interest for perennial crops such as trees, and for climatological studies. Logically, the region of low frost risk decreases from January to March (from 6114 to 2189 km^2, i.e. a 64% fall), while the region with a 50/50 frost risk increases during the same period (from 83 522 to 100 923 km^2, i.e. a 21% rise). March is significantly colder than February or January, as the winter half of the year approaches. But frost in January or in the beginning of February is catastrophic for production. On the whole, only a small part of the Altiplano, 2020 km^2, presents a very low risk of frost during the period January–March. These results underline the major limitation of agriculture on the Bolivian Altiplano by frosts.

6.2. Influence of relief

One fact does not appear immediately on the maps, but those who know the Altiplano may note that the warm regions often correspond to hills. It is well known that slopes are warmer than flat open country: since cold air is denser it flows down from the hills on to the plains (Antonioletti, 1988; Collier et al., 1989; Lagouarde et al., 1983).

This is demonstrated in Fig. 6, which is an enlargement of the upper rectangle in Fig. 5 showing the Corocoro hills zone, plotted with relief contour lines. It is clear that each hill on the relief contour lines map is characterised by an increase of temperature: Fig. 6 shows warm hills on the left side (from north to south: Cerro Chojlluma, Cerro Antaquira, Cerro Kiburi, Cerro Khasca,. . ., Cerro Nina Kkollu) and cold plains on the right side (from north to south: Chojna Kkollu pampa, Thola Thia pampa, Sirca pampa,. . ., Papel pampa). One may observe that when the altitude of the hill reaches a certain value, the tendency changes: the temperature decreases again due to the high altitude. For instance, it is interesting to note, in the south, that the yellow zone of Cerro Huayllokho (4586 m) is colder than the hillsides in orange, but warmer than the plains.

The few orange pixels in the north, which are not related to hills, belong to a river, called the Desaguadero, crossing the region from west to east: this river contains water in February, and thus appears warmer than the surroundings. Just below the Desaguadero river, in the east, another region of interest is the right zone of the map with the warmer yellow zones near Colque Amaya and Papel Pampa. When compared with land-use map, one notes that these yellow zones correspond to saline/sodic soils with halophytic plants (*janquial–junellia*). Moreover, these warmer zones are used as pastoral and crop areas (potatoes and quinua), which correspond well with the predicted minimum temperatures: between −3°C and −2°C. Further studies have to be made to link the soil-type with the temperature: for instance, one could link the high thermal conductivity of saline/sodic soils with their higher temperatures.

Fig. 7 shows the frost risks for potatoes in February for the area indicated by the lower rectangle in Fig. 5.

Each colour corresponds to a given frost risk margin. This picture shows the high sensitivity of frost risk to relief: the slopes of the two volcanoes are clearly warmer than the surrounding flat open country. These mountains in the middle of the plain cause an immediate reduction of frost risk in their vicinity (from a 100% frost risk to a frost risk lower than 20%). Above a given altitude, the temperature decreases again to reach cold values, and frost risk reaches values greater than 77% again. It is interesting to note that, thanks to the classification and computation of function g, these volcanoes appear on the figure although no classification station is in their vicinity. It is also interesting to find the shape of Cerro Culloma at the north of the map, or the course of the rivers Rio Cosapa, Rio Turco and Rio Lauca on what is no more than a synthesis image.

Therefore, it appears that the resulting products, synthesis images maps, are in accordance with the geographical and topographical details of the region. However, this verification of the methodology is not a quantitative validation. In the following the necessary validation is performed on two different sets of data: a cross-validation is performed on the stations originally used in the scheme, and another validation is performed using new stations, in another region of the Altiplano (see Fig. 1).

6.3. Cross-validation using the original meteorological stations

In order to test the scheme prediction skill for frost statistics products, the cross-validation procedure described in Section 5.3.2 is performed again, using historical data records. For each of the 12 stations the five frost statistics products are calculated (extreme minimum temperatures, average minimum temperatures, frost risk percentages for potatoes, resistant potatoes and quinua). The estimated products are compared with the observed ones (using the historical data record of the deleted station). Three values are calculated corresponding to the 3 months of January, February and March. Therefore, each resulting product are validated using 12 stations $\times$ 3 months $=$ 36 points of data. Results are given in Table 8: for each product, the bias and standard error between the estimated values and the observed ones are given.

Table 8
Comparison of predicted against measured frost risks using historical records

	Bias	SE
Extreme minimum temperature (°C)	0.3	2.3
Average minimum temperature (°C)	−0.1	0.7
Frost risks for potatoes (%)	−0.3	8
Frost risks for resistant potatoes (%)	−0.7	6
Frost risks for quinua and bitter potatoes (%)	0.4	3

Each station has been deleted in turn and the minimum temperatures and frost risks for that station have been predicted for the past 30 years. Twelve stations have been tested for the months of January, February and March (36 data points for each line). For each prediction the bias and the standard error between the estimated and observed values are given.

At first sight, the agreement between real and estimated data is very good except in the first case, corresponding to extreme minimum temperatures: the bias is just fair (0.3°C) and the standard deviation is important (2.3°C). It is normal to observe a larger dispersion with these data since they are very dependent on the dataset used to derive them: for each pixel, only one point of the historical dataset is used to obtain the extreme temperature (which, for instance, is not the case with average temperatures). Therefore, two datasets with a different number of records may not give the same extreme temperature if one of the dataset includes an especially cold year.

On the other hand, the correlation between estimated and real average minimum temperatures is very satisfactory: a bias of −0.1°C and a standard error of 0.7°C. Concerning the frost risk percentages, the results are good for both types of potatoes and quinua: a bias of −0.3, −0.7 and 0.4%, respectively, and standard deviations of 8, 6 and 3%, respectively, for potatoes, resistant potatoes and quinua frost risks. For agriculture, frost risk is much more important than extreme temperatures.

6.4. Validation using new meteorological stations

The stations used for cross-validation are mostly clustered near Lake Titicaca, and no station is in the centre and western part of the Altiplano. In order to perform the validation test of the scheme in this latter region, some not already used stations for the classification and zoning are used as validation stations. We

have at our disposal five additional stations in different zones (see Fig. 1): the stations of Sajama, Salinas, Huachacalla, Tacagua and Pazña. These stations are situated far from any station used for the classification, and therefore it is interesting to see whether the scheme still performs well or not for these cases. These stations have not been used for the scheme determination because the data obtained from these stations are less accurate than the other ones. They were, however, considered as accurate enough to perform a validation test.

This time each resulting product is validated using five stations $\times$ 3 months $= 15$ points of data. We compare the five products (extreme minimum temperatures, average minimum temperatures, frost risk percentages for potatoes, resistant potatoes and quinua) for each station using two methods: directly using the records data of the given station (observations), and using the computed maps (estimated values).

Results of the validation are presented on Fig. 8-Fig. 9. Once again, the correlation between real and estimated data is very good except in the first case of the extreme minimum temperatures, Fig. 8(a), where the correlation is just fair. As explained above, it is normal to observe a larger dispersion with the extreme minimum temperatures which are very dependent on the dataset used to derive them. For instance, the real Sajama dataset includes only 6 years of data, while the Sajama temperature estimations uses the Charaña and Potosi records, including 44 and 47 years of data, respectively. With these reservations, one notes a fair bias of -0.6°C and a rather important standard deviation of 1.7°C.

On the other hand, the correlation between estimated and observed average minimum temperatures is very satisfactory again: a bias of 0.1°C and a standard error of 0.5°C (see Fig. 8(b)). Concerning the frost risk percentages, the results are also good for both types of potato and quinua: a bias of 3, 1.3 and -1%, respectively, and standard deviations of 7, 8 and 7%, respectively, for potatoes, resistant potatoes and quinua frost risks (see Fig. 9).

As a conclusion, both the cross-validation and validation using new stations give comparable results. The scheme may therefore be considered as valid for the whole Altiplano. To summarise, considering both validations, the precision of the method in estimating frost risk on the Altiplano is of the order of 9%, and the precision on the average minimum temperature is better than 0.8°C, bias included.

7. Discussion of future developments

The classification and zoning methods are based on different assumptions that seem to be justified since the estimated results correspond well to observations. Nevertheless, the cross-validation results show that the accuracy of the method is not optimal.

One of the most important limitations of the precision of the method is the assumption made in Section 5.2 that f may identify with f' for given zones: this seems intuitively correct, and the results give confidence in this assumption, but no real demonstration is given. The cross-validation techniques performed in Section 5.3.2 give an estimate of 1.5°C for the error in this part when the whole scheme is considered, but the separate theoretical error in f reaches 2°C. Therefore the determination of f should be improved in future. This point will be investigated in order, either to give a rigorous justification to the assumption made to derive f from f', or to find another formulation. Early 5 and 6 a.m. images will be used, combined with simple analytical frost predicting models (such as presented in Figuerola and Mazzeo, 1997) and linked to the results obtained in similar studies (Santibañez et al., 1998). At the same time, from a physical point of view, it may be interesting to investigate carefully the cooling mechanisms of the Altiplano: the role of the slopes has been pointed out here, but other factors are of importance, like type of soil, etc. Here again, the use of frost-predicting models may be appropriate to this purpose.

Another limitation in the scheme is the consequence of the uncertainty in the correlation that is obtained in the derivation of function f' (0.9°C, see Table 3, Section 4). It is clear that the results are dependent on the number of satellite images used to perform the correlation with the station data: more images, over a longer period, would allow a better correlation and better determination of f', and therefore of f.

Concerning the spatial aspect, it is to be expected that a greater number of stations would improve the determination of g' and also the accuracy of f. Moreover, the patchiness of the assigned zones in Fig. 4 suggests that better temperature specification could be

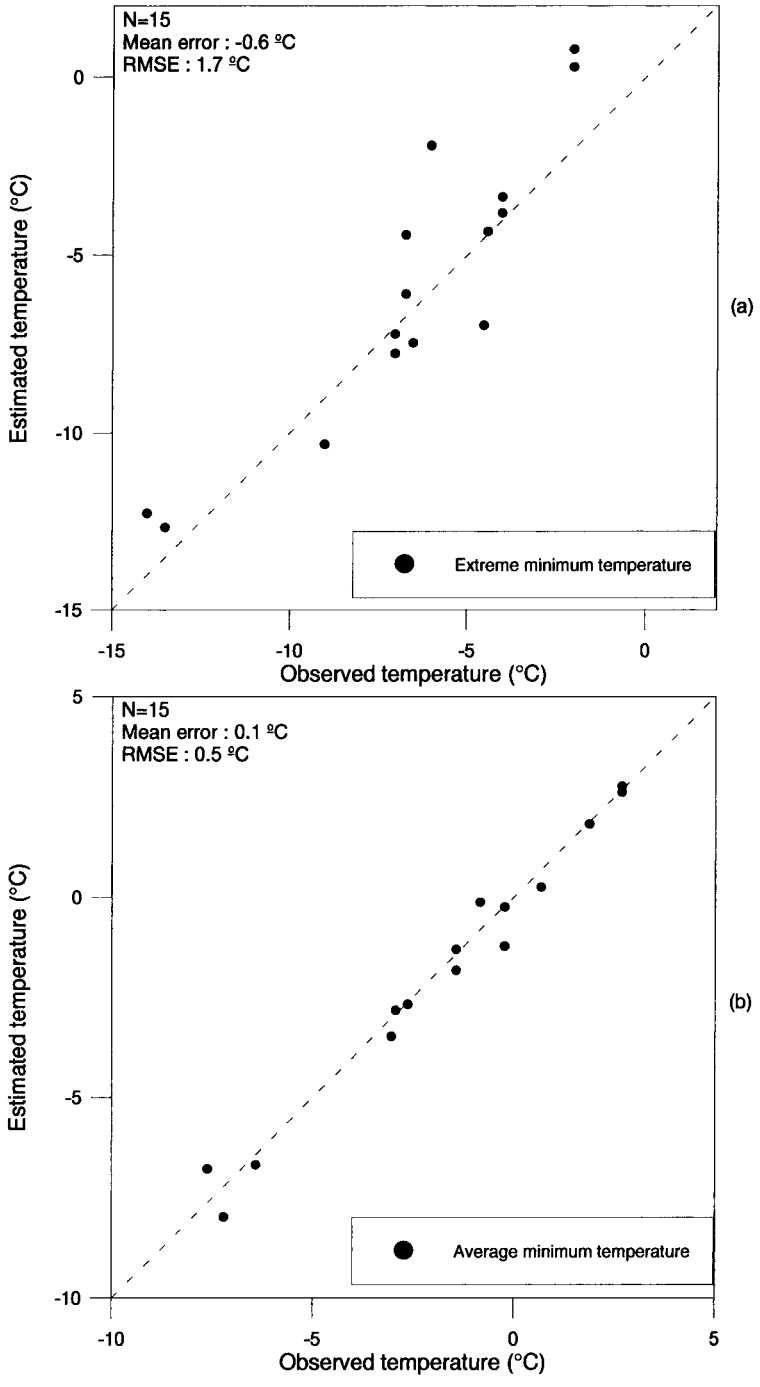

Fig. 8. Comparison between observed and estimated temperatures at the validation stations (see Fig. 1(a) extreme and (b) average minimum temperatures.

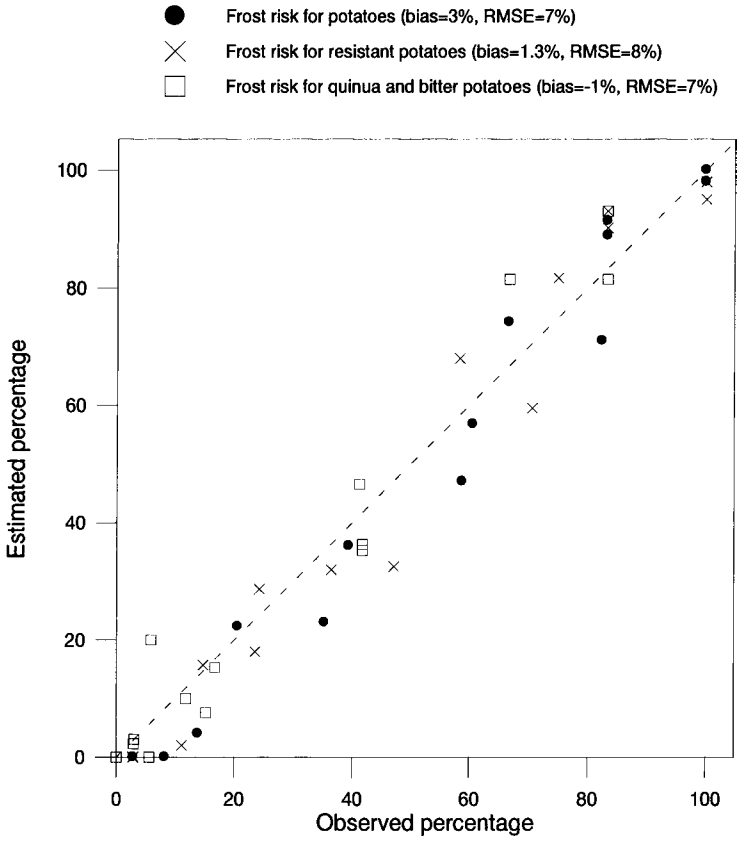

Fig. 9. Comparison between observed and estimated frost risks at the validation stations (see Fig. 1): (i) potatoes, (ii) resistant potatoes and (iii) quinua and bitter potatoes.

achieved if the regressions were to use multiple stations as predictors. This should significantly improve the accuracy of both g' and f, without the need of new stations.

Finally, some stations have limited historical records (i.e. 10 years of data), and must be used with care in this classification.

From a modelling point of view, the method developed in this work may be adapted to quantities other than temperatures. In this study a physical quantity, namely, the minimum air temperature, is related to a remote sensing parameter, namely, the satellite surface temperature. One can imagine that other related quantities may be linked so that one can spatially extrapolate point meteorological data using remote sensing data. This method, using both in situ and remote sensing data, may be seen as an alternative to determine physical quantities that are difficult to measure directly. For instance, if one can find a remote-sensed parameter related to evapotranspiration (like the difference between surface and mid-day air temperatures), it may be possible to derive evapotranspiration for a whole region using data from a few stations measuring real evapotranspiration. Another example could be the measurement of LAI using the vegetation index (NDVI). The condition is to have a good enough temporal correlation between the two parameters during a given period, and a representative number of in situ data.

The influence of each station in zoning has been studied. It seems possible to keep good accuracy in frost risk estimations with relatively few stations if they are chosen with care. But in the frame of this study, it has not been necessary to reduce the number of used stations. In the future, however, this could be useful since some stations are documented with daily

data. If feasible, using multiple stations as predictors for instance, zoning including only the stations documented with daily data would offer additional possibilities to refine the study: for instance, it would be interesting to work directly on daily data to compute the probability for having a given period free of frost (90 and 120 days, depending on the cultivation). One could also calculate the length of frost-free periods with different levels of probability. Such frost frequency studies are only possible with daily data.

8. Concluding remarks

In this study, a frost risk zoning for the Bolivian Altiplano has been developed using different spatial functions to make the link between the 2 a.m. surface satellite temperatures and the 6 a.m. minimum air station temperatures. Five types of maps (or synthesis images) are thus derived: an extreme minimum temperature map, an average minimum temperature map, and three frost risk percentages maps for potatoes (-2°C), resistant potatoes (-3°C) and quinua (-5°C).

The minimum temperatures appear to be related to the slopes and the hills where the temperatures are warmer than in the open flat country. Bolivian farmers use terrace cultivation on hillsides all over the Altiplano for frost-sensitive crops. In the case of mountains or volcanoes, the slope temperature decreases again above a given altitude, and is naturally very cold at the top of the mountains.

The accuracy obtained with the classification zoning method is better than 0.8°C for the average minimum temperatures, and better than 9% for the frost risk percentages, with a very low bias in both cases. The extreme minimum temperatures are less accurately estimated, but this is a bias of the validation method and not a real limitation of the estimate: further validation should be performed to estimate in this case the accuracy of the method more correctly.

This method, with its limitations, proves to work efficiently for the frost study, and the resulting frost risk maps may be used by the Bolivian authorities to develop frost risk protection plans in the regions where risks for crops exist. These maps may be used at different scales: from regional (Fig. 5) to local (Figs. 6 and 7) scale, according to needs.

This study also demonstrates that apart from the particular application to frost risks, it is possible to develop a method that combines satellite and meteorological station data to derive information that is not present in the original data.

For the future, studies of frost frequency using daily data, and assimilation in frost prediction models are planned.

Acknowledgements

The authors are grateful to Fernando Santibañez (Chile) for fruitful discussions about the original idea of the classification method developed in this study. This study has been carried out in the framework of a scientific cooperation with the ABTEMA (Asociacion Boliviana de Teledeccion para el Medio Ambiente) and the SENAMHI (Servicio Nacional de Meteorologia e Hydrologia de Bolivia) which provided us with meteorological station data. This work was funded by the European contract ERBTS CT930239 'Climatological and Hydrological Determinants of Agricultural Production in South America: Remote Sensing and Numerical Simulation.' The authors are very grateful for fruitful suggestions and remarks by anonymous reviewers who helped to considerably strengthen the original manuscript.

Appendix A

Estimation of the error due to the assumption of a constant emissivity

We have assumed that no important temporal variation of the surface emissivity ε in the spectral band [10–12 μm] was to occur on the Altiplano, and therefore a constant surface emissivity has been chosen ($\varepsilon = 1$) for all pixels and all images. However, in general, the emissivity of a given pixel may change throughout the year, from 0.92–0.93 for bare soil to 0.99 for a fully vegetated area. The important feature here is not the absolute value of emissivity (since the satellite-derived temperatures are then correlated to air temperatures), but its temporal variations, which could damage the correlation.

The error in T_s due to an error in ε is linearly related to T_s; for average climatic conditions $\Delta T_s \approx 60$

$\Delta\varepsilon$(François and Ottlé, 1996), (see also Becker, 1987, who gives a similar expression). In the following, a specific calculation for the conditions of the Altiplano is presented.

The surface brightness radiance obtained after atmospheric correction, but before emissivity correction is:

$$B_\lambda(T_b) = \varepsilon B_\lambda(T_s) + (1-\varepsilon)R_a \qquad (A.1)$$

where B_λ is the Planck function for a given wavelength λ, R_a is the atmospheric downward radiance for the same wavelength, ε the actual surface emissivity and T_b the surface brightness temperature.

The Planck function B_λ may be linearized around the [260 K → 283 K] region (e.g.) at $\lambda = 11\,\mu m$ (AVHRR channel 4):

$$B_{11}(T_b) \approx 1.31T_b - 281.3 \qquad (A.2)$$

(with T_b in Kelvin and B in W/m^2 at 11 μm)

A simple calculation gives a general formulation of the difference $\Delta T_s = T_b - T_s$:

$$\Delta T_s \approx \Delta\varepsilon(T_s + 58 - R_a/1.3) \qquad (A.3)$$

(with T_s in °C and R_a in W/m^2 at 11 μm).

At 11 μm, R_a varies over the range 40 W/m^2 (clear cold sky conditions: −30°C) to 90 W/m^2 (cloudy sky: 10°C). Applying (Eq. (A.3)) for some average conditions ($T_s = 15$°C, $R_a = 17$ W/m^2), gives the expression cited in François and Ottlé (1996):

$$\Delta T_s \approx 60\Delta\epsilon \qquad (A.4)$$

Applying Eq. (A.3) for the specific conditions of the Altiplano (-20°C $< T_s < 10$°C, $R_a = 40$ W/m^2), gives a more favourable expression:

$$7\Delta\varepsilon < \Delta T_s < 37\Delta\varepsilon \qquad (A.5)$$

Therefore a variation of 0.02 in the emissivity during the year would lead to a typical variation between 0.1°C and 0.7°C in the surface temperature derived from satellite.

Appendix B

Determination of linear spatial functions f, f', g and g':

Let us call f' the function which relates T_s to T_{min} for each station:

$$T_s(x_i, y_i) - - - - - f' - - - - - \rightarrow T_{min}(x_i, y_i)$$

where (x_i, y_i) is the position of the ith station. For each station i, f' may be parameterized as

$$T_{min}(x_i, y_i) = a'(i)T_s(x_i, y_i) + b'(i) \qquad (B.1)$$

where i is the number of the station, (x_i, y_i) the position of the ith station pixel, and $a'(i)$ and $b'(i)$ are the coefficients attached to ith station.

Function f is the spatial extension of f' : f relates T_s to T_{min} for each pixel (x, y), and no longer for each station:

$$T_s(x, y) - - - - - f - - - - - \rightarrow T_{min}(x, y)$$

For each pixel (x, y), f may be parameterised as

$$T_{min}(x, y) = a(x, y)T_s(x, y) + b(x, y) \qquad (B.2)$$

where (x, y) is the position of a pixel on the Altiplano, and $a(x, y)$ and $b(x, y)$ the coefficients attached to this pixel to relate T_s to T_{min}.

The problem is, assuming f' is known, how could we obtain f. The solution is a classification of the Altiplano: since we cannot use a global relation for the whole Altiplano, we use 17 relations applied to 17 *zones*, corresponding to the 17 meteorological stations. The problem is to determine these zones (which need not be continuous). This is done introducing a new function g', relating the surface temperature of the ith station $T_s(x_i, y_i)$ to whatever pixel $T_s(x, y)$:

$$T_s(x_i, y_i) - - - - - g' - - - - - \rightarrow T_s(x, y)$$

This function relates every pixel (x, y) to the station pixel (x_i, y_i). For each zone i, and for each pixel (x, y) belonging to i, g' may be parameterised as:

$$T_s(x, y) = \alpha'(x, y)T_s(x_i, y_i) + \beta'(x, y) \qquad (B.3)$$

where i is a zone centred on station (x_i, y_i), and (x, y) is a pixel over the Altiplano belonging to i, $\alpha'(x, y)$ and $\beta'(x, y)$ being the coefficients attached to this pixel.

The problem is to find to what station should be attached a given pixel (x, y). This is done for each pixel (x, y) and all the AVHRR images by calculating the coefficients α' and β' for all the 17 stations. The station giving the best correlation coefficient is kept, and attached to the pixel (x, y), as well as the corresponding coefficients α' and β'. More details are given in Section 5.1.

This method allows us to classify the whole Altiplano according to the stations. Function g' actually

also allows to compute the whole map of *satellite* temperatures knowing only the 17 *satellite* temperatures at the stations. However, it would be more useful for our purpose to be able to compute *minimum* temperatures over the whole Altiplano knowing the 17 *minimum* temperatures at the stations. This is the role of function g, which is the equivalent of g', but in terms of minimum air temperatures:

$$T_{\min}(x_i, y_i) - - - - - g - - - - - \rightarrow T_{\min}(x, y)$$

This function relates the minimum temperature of every pixel (x, y) to that of the station (x_i, y_i). For each zone i, and for each pixel (x, y) belonging to i, g may be parameterised as:

$$T_{\min}(x, y) = \alpha(x, y) T_{\min}(x_i, y_i) \beta(x, y) \qquad \text{(B.4)}$$

where (x, y) is a pixel over the Altiplano belonging to zone i, and $\alpha(x, y)$ and $\beta(x, y)$ are the coefficients attached to this pixel.

From the above definitions, it is easy to show that $g = f\ (g'(f^{-1}))$: let us consider a pixel (x, y) that belongs to the zone of station i: it appears that one can determine its minimum temperature $T_{\min}(x, y)$ from the minimum temperature $T_{\min}(x_i, y_i)$ measured at station i :

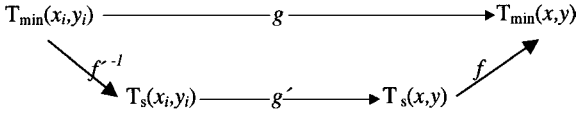

which can be written as:

$$g = f(g(f^{-1})) \qquad \text{(B.6)}$$

The hypothesis made in Section 5.2 is that $f = f'$, and therefore (Eq. (A.5)) writes as

$$g = f(g(f^{-1})) \qquad \text{(B.7)}$$

Or equivalently:

$$g(T_{\min}(x_i, y_i)) = a\left[\alpha'\left(\frac{T_{\min}(x_i, y_i) - b}{a}\right) + \beta'\right] + b \qquad \text{(B.8)}$$

which becomes

$$T_{\min}(x, y) = g(T_{\min}(x_i, y_i)) = \alpha' T_{\min}(x_i, y_i) - \alpha' b + a\beta' + b \qquad \text{(B.9)}$$

One may note, looking at (Eq. (B.9)) that g is close, but not equal to g': the difference lies in the constant term that is different from β'. Therefore, the determination of f, f' and g' is needed to be able to calculate function g, which is the function that permits spatial extension of the historical minimum temperature data records.

References

Allirol, G., Bosseno, R., Vacher, J.J., 1992. Primeros ensayos de zonificación de las heladas en el Altiplano Boliviano con el uso del infrarojo térmico del satélite NOAA-AVHRR, Proc. Reunion Regional sobre el uso y procesamiento digital de imágenes, Instituto Geográfico Agustin Codazzi (IGAC), Bogota de Santa Fe, 9–11 December 1992, Cipres review from IGAC, 15, 1992, pp. 57–64.

Antonioletti, R., 1988. Délimitation des zones à risques de gel à l'aide de thermographies infrarouges satellitaires. Publications de l'Association Internationale de Climatologie 1, 41–46.

Becker, F., 1987. The impact of spectral emissivity on the measurement of land surface temperature from a satellite. Int. J. Remote Sens. 8, 1509–1522.

Cellier, P., 1989. Mécanismes du refroidissement nocturne. Application à la prévision des gelées de printemps, Proc. Le gel en Agriculture, Paris, France, 21–22 November 1989, pp. 145–164.

Collier, P., Runacres, A.M.E., McClatchey, J., 1989. Mapping very low surface temperature in the Scottish Highlands using NOAA AVHRR data. Int. J. Remote Sens. 10(9), 1519–1529.

Du Portal, D., 1993. Etudes des gelées sur l'Altiplano Bolivien, M.S. report, Montpellier, France, 40 pp.

François, C., Ottlé, C., 1996. Atmospheric corrections in the thermal infrared: Global and water-vapour dependent Split-Window algorithms: Application on ATSR data. IEEE Trans. Remote Sens. 34(2), 457–470.

Figuerola, P.I., Mazzeo, N.A., 1997. An analytical model for the prediction of nocturnal and dawn surface temperatures under calm, clear sky conditions. Agric. For. Meteorol. 85, 229–237.

Kerdiles, H., Grondona, M., Rodriguez, R., Seguin, B., 1996. Frost mapping using NOAA AVHRR data in the Pampean region, Argentina. Agric. For. Meteorol. 79, 157–182.

Lagouarde, J.P., Valery, P., Belluomo, P., Soulier, M.A., 1983. Cartographie des topoclimats forestiers. Mise au point d'une méthodologie d'analyse de l'effet du relief sur les thermographies: Application aux données HCMM sur le Nord–Est du Massif Central. Agronomie 3(10), 1011–1018.

Le Tacon, P., 1989. Manifestation des risques climatiques à l'échelle de l'exploitation agricole – Conséquences sur les pratiques paysannes – Cas de l'Altiplano bolivien, Ingenior thesis ENSSAA – CNEARC, 164 pp.

Le Tacon, P., Vacher, J.J., Eldin, M., Imaña, E., 1992. Los riesgos de heladas en el Altiplano Boliviano. Proc. VII Congreso sobre los cultivos andinos, La Paz, Bolivia, pp. 287–292.

Michaelsen, J., 1987. Cross-validation in statistical climate forecast models. J. Clim. Appl. Meteorol. 26, 1589–1600.

Ottlé, C., Outalha, S., Fran, , çois, C.Le Maguer, S., 1997. Estimation of total water vapor content from Split-Window radiance measurements. Remote Sens. Environ. 61, 410–418.

Santibañez, F., Morales, L., Cellier, P., 1998. Predicting minimum temperatures at regional scales in the central valley of Chile, Agronomie, in press.

Saunders, R.W., Kriebel, K.T., 1988. An improved method for detecting clear sky and cloudy radiances from AVHRR data. Int. J. Remote Sens. 9(1), 123–150.

Seguin, B., Baeltz, B., Favard J.C., Mandeville, J.C., Monget, J.M., 1981. Signification de la thermographie I. R. par satellite en agroclimatologie dans le Sud-Est de la France, Proc. Colloque Int. sur les signatures spectrales d'objets en télédétection, Avignon, France, 8–11 September 1981, pp. 467–476.

Sobrino, J.A., Li, Z.L., Stoll, M.P., Becker, F., 1993. Improvements in the Split-Window technique for land surface temperature determination. IEEE Trans. Remote Sens. 32(2), 243–253.